

A scaling approach for quantifying the net CO₂ flux of the Kuparuk River Basin, Alaska

WALTER C. OECHEL,* GEORGE L. VOURLITIS,*† JOSEPH VERFAILLIE JR.,†
TIM CRAWFORD,‡ STEVE BROOKS,‡ EDWARD DUMAS,‡ ALLEN HOPE,§
DOUGLAS STOW,§ BILL BOYNTON,§ VIKTOR NOSOV* and ROMMEL ZULUETA
**Global Change Research Group, Department of Biology, San Diego State University, San Diego, CA 92182, †Biological Sciences Program, California State University, San Marcos, CA 92096-0001, ‡NOAA Atmospheric Turbulence and Diffusion Division, Oak Ridge, TN 37831, §Department of Geography, San Diego State University, San Diego, CA 92182, USA*

Abstract

Net CO₂ flux measurements conducted during the summer and winter of 1994–96 were scaled in space and time to provide estimates of net CO₂ exchange during the 1995–96 (9 May 1995–8 May 1996) annual cycle for the Kuparuk River Basin, a 9200 km² watershed located in NE Alaska. Net CO₂ flux was measured using dynamic chambers and eddy covariance in moist-acidic, nonacidic, wet-sedge, and shrub tundra, which comprise 95% of the terrestrial landscape of the Kuparuk Basin. CO₂ flux data were used as input to multivariate models that calculated instantaneous and daily rates of gross primary production (GPP) and whole-ecosystem respiration (R) as a function of meteorology and ecosystem development. Net CO₂ flux was scaled up to the Kuparuk Basin using a geographical information system (GIS) consisting of a vegetation map, digital terrain map, dynamic temperature and radiation fields, and the models of GPP and R.

Basin-wide estimates of net CO₂ exchange for the summer growing season (9 May–5 September 1995) indicate that nonacidic tundra was a net sink of -31.7 ± 21.3 GgC (1 Gg = 10⁹ g), while shrub tundra lost 32.5 ± 6.3 GgC to the atmosphere (negative values denote net ecosystem CO₂ uptake). Acidic and wet sedge tundra were in balance, and when integrated for the entire Kuparuk River Basin (including aquatic surfaces), whole basin summer net CO₂ exchange was estimated to be in balance (-0.9 ± 50.3 GgC). Autumn to winter (6 September 1995–8 May 1996) estimates of net CO₂ flux indicate that acidic, nonacidic, and shrub tundra landforms were all large sources of CO₂ to the atmosphere (75.5 ± 8.3 , 96.4 ± 11.4 , and 43.3 ± 4.7 GgC for acidic, nonacidic, and shrub tundra, respectively). CO₂ loss from wet sedge surfaces was not substantially different from zero, but the large losses from the other terrestrial landforms resulted in a whole basin net CO₂ loss of 217.2 ± 24.1 GgC during the 1995–96 cold season. When integrated for the 1995–96 annual cycle, acidic ($66.4 + 25.25$ GgC), nonacidic (64.7 ± 29.2 GgC), and shrub tundra (75.8 ± 8.4 GgC) were substantial net sources of CO₂ to the atmosphere, while wet sedge tundra was in balance ($0.4 + 0.8$ GgC). The Kuparuk River Basin as a whole was estimated to be a net CO₂ source of 218.1 ± 60.6 GgC over the 1995–96 annual cycle. Compared to direct measurements of regional net CO₂ flux obtained from aircraft-based eddy covariance, the scaling procedure provided realistic estimates of CO₂ exchange during the summer growing season. Although winter estimates could not be assessed directly using aircraft measurements of net CO₂ exchange, the estimates reported here are comparable to measured values reported in the literature. Thus, we have high confidence in the summer estimates of net CO₂ exchange and reasonable confidence in the winter net CO₂ flux estimates for

terrestrial landforms of the Kuparuk river basin. Although there is larger uncertainty in the aquatic estimates, the small surface area of aquatic surfaces in the Kuparuk river basin ($\approx 5\%$) presumably reduces the potential for this uncertainty to result in large errors in basin-wide CO₂ flux estimates.

Keywords: Arctic, global change, ecophysiology, eddy covariance, trace-gas flux, tundra

Introduction

High-latitude climate change has led to substantial changes in arctic ecosystem structure and function over the last four decades (Grulke *et al.* 1990; Oechel *et al.* 1993, 1995; Oechel & Vourlitis 1994, 1995; Chapin *et al.* 1995; Tenhunen *et al.* 1995). This observation is based primarily on results from plot-scale experimental and observational studies, which have been instrumental in elucidating the mechanistic response of arctic tundra ecosystems to climate change. However, the potential regional- and global-scale feedbacks associated with the recent climate change-induced alteration in arctic system CO₂ flux are uncertain (Oechel & Vourlitis 1994; Weller *et al.* 1995; Baldocchi *et al.* 1996) because the heterogeneous nature of arctic landscapes limits our ability to generalize plot- and local-scale information. Thus, regional estimates of net CO₂ flux are required for understanding and predicting the response of arctic Alaska to climate change and for assessing the role of Alaskan arctic tundra ecosystems in the global atmospheric CO₂ budget (Oechel & Vourlitis 1994; Weller *et al.* 1995; Baldocchi *et al.* 1996).

Simulation models provide a means for assessing large-scale ecosystem function (Raich *et al.* 1991; VEMAP 1995; Williams *et al.* 1997). However, simulation approaches are problematic because the structural and functional input variables required to parameterize these complex models (e.g. stem area density, plant nutrient uptake, etc.) are not available for whole regions and/or their spatial variance across regions is unknown (Raich *et al.* 1991; Williams *et al.* 1997). Furthermore, the regional net CO₂ flux database required to validate flux estimates from simulation models is lacking (Raich *et al.* 1991; VEMAP 1995; Williams *et al.* 1997). Thus, simulation results can only be viewed as a complex hypothesis until validated with regional data (Rastetter 1996).

As part of the National Science Foundation's, Arctic-Systems-Science, Land-Atmosphere-Ice-Interactions (NSF-ARCSS-LAI) flux study (Weller *et al.* 1995), we quantified the spatial and temporal patterns of net CO₂ flux between 1994 and 1995 using chamber and tower-based eddy covariance measurement techniques (Vourlitis *et al.* 1993; Vourlitis & Oechel 1997, 1999). Using this spatially explicit database, we developed physiological-based models to link the variations in net CO₂ flux to fluctuations in meteorology, hydrology, and

phenology (Hope *et al.* 1995; McMichael 1995; Vourlitis & Oechel 1997, 1999; McMichael *et al.* 1999; Vourlitis *et al.*, in press a & b). Here we describe a method for the spatial and temporal scaling of plot (0.5 m²) and hectare (0.5–3 ha) measurements of net CO₂ flux to provide estimates of CO₂ exchange for the Kuparuk River Basin for the 1995–96 annual cycle (9 May 1995–8 May 1996), a 9200 km² watershed located in NE Alaska (Weller *et al.* 1995; Auerbach & Walker 1995; Auerbach *et al.* 1997). Regional net CO₂ flux estimates were derived for the 1995 summer growing season and 1995–96 annual cycle, and the performance of our scaling procedure was assessed using the NOAA-Atmospheric Turbulence and Diffusion Division (NOAA-ATDD) Long-Ez Mobile Flux Platform (MFP) (Crawford *et al.* 1990, 1996; Crawford & Dobosy 1992).

Methods

Field measurements

Field measurements of net CO₂ flux were made during the 1994–95 growing seasons (between 1 June and 31 August) in Alaskan moist-acidic (Happy Valley: 69°09'N, 148°51'W), moist nonacidic (24-Mile: 69°56'N, 148°49'W), shrub (Happy Valley) and wet-sedge tundra ecosystems (U-Pad: 70°17'N, 148°53'W) (Fig. 1). Combined, these ecosystem types comprise approximately 95% of the terrestrial landscape of the Kuparuk River Basin (Auerbach & Walker 1995; Auerbach *et al.* 1997). Measurements were made using portable flux chambers and tower-based eddy covariance techniques, and details of the sampling procedure and research sites are described thoroughly elsewhere (Vourlitis *et al.* 1993; Vourlitis & Oechel 1997, 1999). During the growing season (9 May–5 September), net CO₂ flux measurements for shrub tundra were made using portable chambers (Vourlitis *et al.* 1993; Oechel *et al.* unpubl. data), while data for moist-acidic, nonacidic, and wet sedge tundra were derived from tower-based eddy-covariance measurements (Vourlitis & Oechel 1997, 1999). Winter flux data (6 September–8 May) were derived from chamber measurements (Oechel *et al.* 1997). Net CO₂ flux and whole ecosystem respiration (*R*) was measured directly using the portable chambers (Vourlitis *et al.*

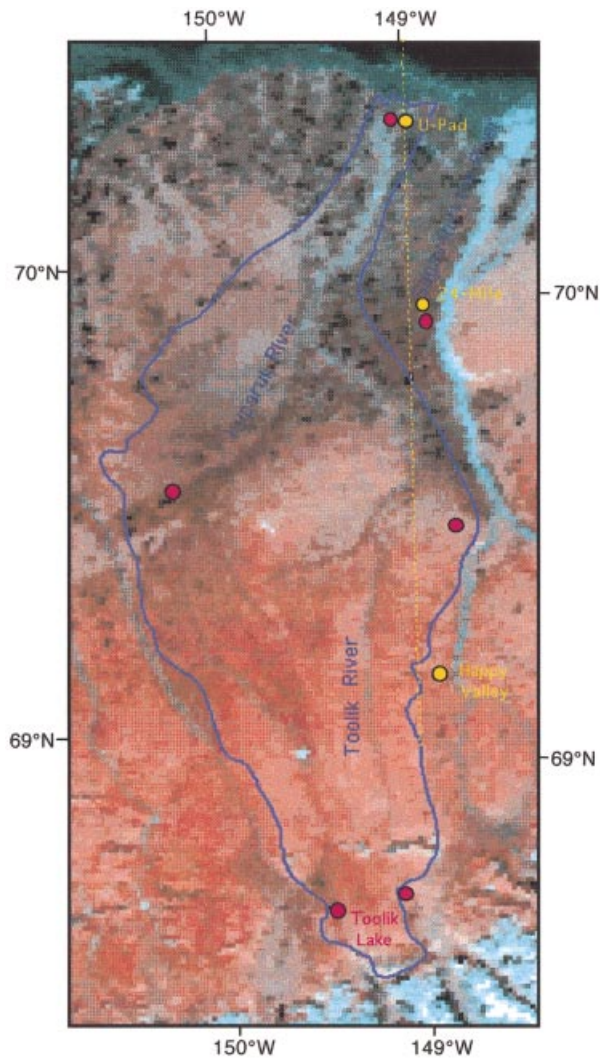


Fig. 1 A false-colour image of the Kuparuk River Basin (solid blue line) obtained from NOAA-Advanced Very High Resolution Radiometer (AVHRR) satellite imagery. Also shown is the location of the net CO₂ flux measurement sites (yellow circles), the 148°55'W latitudinal flux transect flown by the NOAA-Mobile Flux Platform (MFP) (dashed yellow line), and the location of the meteorological measurement sites used for the spatially distributed radiation and temperature maps (red circles).

1993). With eddy covariance, however, R was assumed to be equivalent to night-time net CO₂ flux (F_n) when photosynthetic photon flux density (Q) was $< 50 \mu\text{mol m}^{-2}\text{s}^{-1}$ and wind speed was $> 2 \text{ m s}^{-1}$ (Ruimy *et al.* 1995; Vourlitis & Oechel 1999; Vourlitis *et al.*, 2000a). Gross primary production (GPP) was calculated as the difference between R and net CO₂ flux.

Scaling procedure

Physiologically based models were used to temporally scale the measured and estimated R and GPP (Vourlitis

et al. 2000b). The flux and meteorology data (radiation and temperature) obtained from the field measurements were input to nonlinear models which calculated instantaneous (30 minute average) and daily rates of GPP and R (Fig. 2). Instantaneous rates of GPP were estimated as a hyperbolic function of shortwave radiation (Q),

$$\text{GPP} = \frac{aQb}{aQ + b} \quad (1)$$

(Thornley 1976). Instantaneous rates of R (and F_n) were estimated as an exponential function of air temperature (T°),

$$R = a \exp(bT^\circ) \quad (2)$$

(Peterson & Billings 1975; Billings *et al.* 1977; Bunnell *et al.* 1977; Oechel *et al.* 1995). Daily rates of GPP were calculated as a sigmoidal function of the normalized difference vegetation index (NDVI) and a hyperbolic function of average daily Q .

$$\text{GPP} = \left[\frac{a}{1 + \exp(b - c\text{NDVI})} \right] \left[\frac{dQe}{dQ + e} \right] \quad (3)$$

The NDVI was calculated from NOAA-Advanced Very High Resolution Radiometer (AVHRR) satellite imagery as a bi-monthly composite to screen out periods of cloud cover and poor atmospheric conditions (Williams & Hall 1993). Seasonal NDVI composites were obtained for the 1994 growing season (Fig. 3a) and normalized to vary between 0 and 1 with the peak season value equal to 1 (Fig. 3b). The NDVI is sensitive to seasonal fluctuations in biophysical variables such as biomass, leaf area, and chlorophyll content (Hope *et al.* 1993, 1995; McMichael *et al.* 1999), and thus, is a useful surrogate for quantifying the seasonal trend in ecosystem development. Daily R was calculated as an exponential function of average daily air temperature using (2). Regression coefficients (a – e) were estimated by nonlinear least-squares regression (SYSTAT, Evanston, IL), and the daily models explained on average 61 and 73% of the daily variance in GPP and R , respectively (Table 1). The daily and instantaneous models were cross-calibrated by applying the daily integrated GPP and R calculated from the instantaneous models (eqns 1 and 2) to the daily models (eqns 2 and 3) (Rastetter *et al.* 1992; Kicklighter *et al.* 1994).

Autumn and winter flux models (6 September–8 May) expressed net CO₂ efflux as an exponential function of soil temperature at 10 cm using (2). The start of winter was defined as the point when the normalized NDVI was < 0.10 (Fig. 2b) and net CO₂ flux was assumed to be driven completely by R (GPP = 0). The intercept of the R

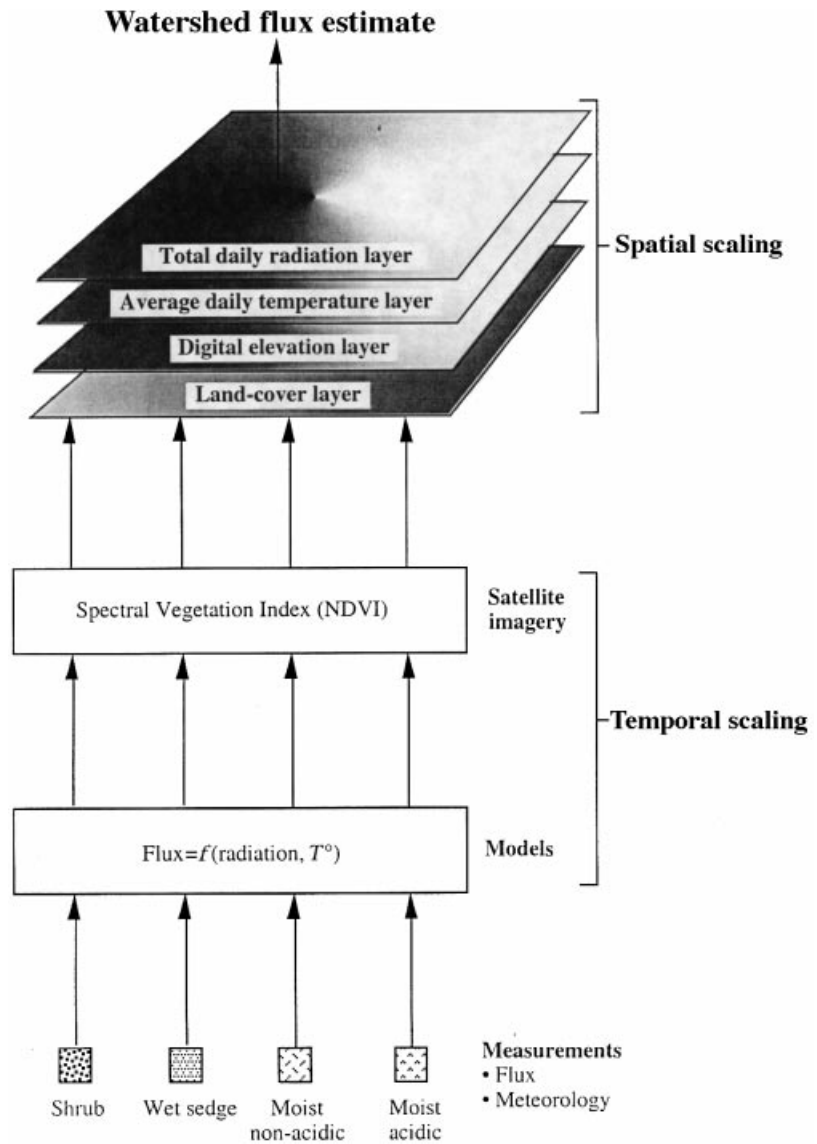


Fig. 2 Flow-chart of the scaling procedure for estimating the net CO₂ flux of the Kuparuk River Basin watershed of NE Alaska. Chamber and eddy covariance measurements of net CO₂ flux, meteorological measurements (radiation and temperature), and satellite imagery (NDVI) were used to parameterize physiological models which represent the temporal scaling component. The Geographic Information System (GIS) consists of land-cover, digital elevation, and dynamic radiation and temperature layers, which combined, represent the spatial scaling component. Linking the temporal (models) and spatial (GIS) scaling components allowed for daily estimates of watershed-scale flux.

vs. temperature function (*a* coefficient, eqn 2) was set to equal the daily *R* estimated for the last day of the summer growing season, while the temperature sensitivity was set at 0.1 gC m⁻² d⁻¹ (*Q*₁₀=2.7) for each terrestrial land-cover type.

The temporally scaled estimate of net CO₂ flux derived from the nonlinear models was spatially scaled to the Kuparuk Basin using a geographical information system (GIS) database consisting of a land-cover (Fig. 1), digital elevation, and dynamic temperature and radiation layers (Auerbach & Walker 1995; Auerbach *et al.* 1997; Hinzman *et al.* 1998) (Fig. 2). The land-cover and elevation layers were geo-referenced and scaled to a common grid size of 300 m². Average daily radiation and temperature layers

were calculated by interpolating (kriging) observed values obtained from six meteorological stations (Hinzman *et al.* 1998) located within the basin domain (Fig. 1). Net CO₂ exchange from barren surfaces (1.4% of the total surface area in the Kuparuk Basin; Auerbach & Walker 1995) was set to zero, and summer aquatic net CO₂ efflux was assumed to equal 25% of the terrestrial net CO₂ exchange (Kling *et al.* 1991).

Summer (9 May–5 September), winter (6 September–8 May), and annual estimates of net CO₂ exchange were calculated for each land-cover type and the entire Kuparuk Basin watershed. Daily models were used to calculate the total daily flux for each 300 m² pixel of the Kuparuk GIS. Daily CO₂ flux for each land-cover type

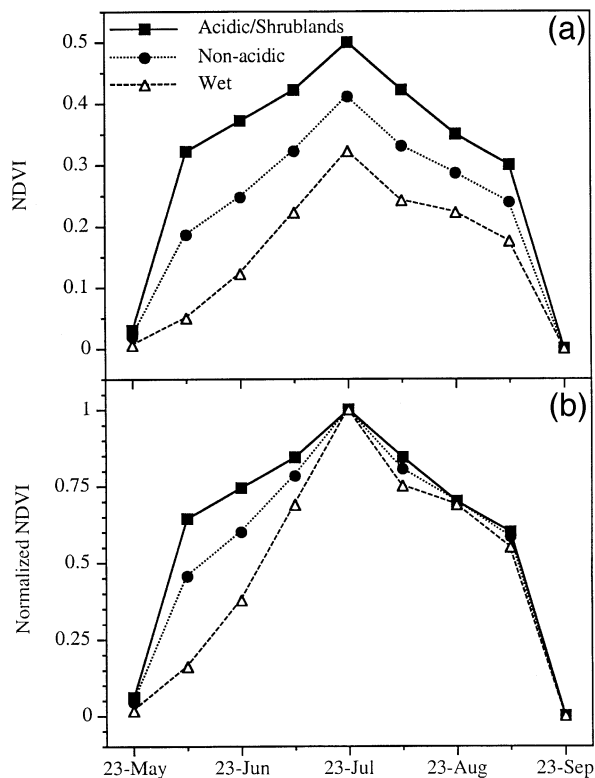


Fig. 3 Seasonal pattern in the Normalized Difference Vegetation Index (NDVI) (a) and the normalized-NDVI (b) calculated from 15 d composites from Advanced Very High Resolution Radiometer (AVHRR) imagery acquired for the Kuparuk River Basin during the 1994 growing season. Data are for acidic and shrub tundra combined (closed squares and solid lines), nonacidic tundra (closed circles and short-dashed lines), and wet sedge tundra (open triangles and long-dashed lines).

was calculated by summing the flux for all pixels representing a given land-cover type, whereas daily CO₂ flux for the entire basin was calculated by summing the flux for all pixels within the Kuparuk River Basin domain. Daily fluxes for each land-cover type and the entire basin were integrated over summer (119 days), winter (246 days), and annual periods and expressed on a per metre and basin-wide basis.

The scaling procedure calculates total fluxes for various land-cover types and for the entire basin. Thus, an estimate of the variance associated with a given seasonal flux estimate cannot be calculated without an extensive sensitivity or error analysis. To provide an estimate of the random variance associated with each seasonal and annual net CO₂ flux estimate, each total daily flux time-series was bootstrapped (Efron & Tibshirani 1993). The bootstrapping technique calculates a standard error using a three-step process. First, the bootstrap constructs several sample data series (for our

Table 1 Daily gross primary production (GPP) and whole-ecosystem respiration (*R*) models (see eqns 2 and 3; Methods) for scaling plot (0.5 m²) and landscape-scale (0.5–3 ha) net CO₂ flux measurements to the Kuparuk River basin during the 1995 growing season. Coefficients and goodness of fit (*R*²) values were estimated using nonlinear, least-squares regression

Landcover type	<i>a</i>	<i>b</i>	<i>c</i>	<i>d</i>	<i>e</i>	<i>R</i> ²
Gross primary production (GPP)						
Acidic	2.04	10.17	13.69	0.74	2.05	0.74
Non-acidic	3.34	3.94	6.14	0.01	0.83	0.41
Shrub	0.72	16.09	20.42	0.04	5.51	0.86
Wet sedge	0.93	7.70	13.14	0.03	2.01	0.77
Whole-ecosystem respiration (<i>R</i>)						
Acidic	1.14	0.06				0.76
Non-acidic	0.61	0.05				0.67
Shrub	1.17	0.07				0.61
Wet sedge	0.22	0.10				0.89

application, 4000 bootstrapped sample data series) by randomly sampling (with replacement) the observed data series (Efron & Tibshirani 1993). Next, a statistic (e.g. average) is calculated from each constructed sample data series (Efron & Tibshirani 1993). Finally, a summary statistic (e.g. a grand mean), and the variability about the summary statistic (e.g. standard error), is calculated from the distribution of averages calculated from the bootstrapped sample data series (Efron & Tibshirani 1993).

To illustrate this procedure, consider the observed summer time-series for acidic tundra surfaces of the Kuparuk River basin, which consisted of 114 estimates (9 May–5 September = 114 d) of the total daily acidic tundra net CO₂ flux calculated from the Kuparuk GIS. Several sample data series (*n* = 4000), each consisting of 114 estimates of the total daily net CO₂ flux, were developed by bootstrapping the observed data series. Each sample data series was constructed by randomly sampling with replacement 114 total daily net CO₂ flux estimates (corresponding to the total length of the time series) from the observed data series. Next, the average total daily net CO₂ flux was calculated for each of the 4000 bootstrapped sample series, and each bootstrapped average was multiplied by the number of days over the summer season (114 d) in order to provide 4000 bootstrapped estimates of the total summer net CO₂ flux for acidic tundra. The average ($\pm 1SE$) total summer net CO₂ flux for acidic tundra was then calculated from the 4000 bootstrapped estimates of the total summer acidic tundra net CO₂ flux, and expressed on a per metre and basin-wide basis. This procedure was repeated for each surface type over summer, winter, and annual periods to

provide an estimate of the variance associated with the estimated net CO₂ flux.

Performance of scaling procedure

The performance of the whole-basin estimation procedure was assessed by aircraft-based eddy covariance measurements of daytime (06.00–18.00 hours) net CO₂ flux derived from the NOAA-Atmospheric Turbulence and Diffusion Division (ATDD) mobile flux platform (MFP) (Crawford *et al.* 1990). Sampling theory and procedures for the NOAA-MFP are described thoroughly elsewhere (Crawford *et al.* 1990; Desjardins *et al.* 1992; Crawford *et al.* 1996; Oechel *et al.* 1998). Measurements were conducted in June 1994 and 1995 and August 1995 over a 200-km long transect located between 68°55' and 70°30'N latitude along the 148°55'W parallel (Figs 1 and 4). The flux transect incorporated the two major physiographic provinces of the Alaskan North Slope, with the foothills region of the Brooks Range in the southern half of the transect and the broad coastal plain in the northern half of the transect (Fig. 1). The aircraft campaigns collected over 200 h of data across a range of weather conditions. Measurements were conducted at an altitude of 10–20 m above ground level; well within the constant flux layer which varied from about 200 m in the early evening to about 500 m in late afternoon (Brooks *et al.* 1997).

To compare the scaled estimates of net CO₂ flux to those measured by the NOAA-MFP, instantaneous models (eqns 1 & 2) were run for each surface type within a 2-km wide belt transect centred on the N–S aircraft flight-line (Fig. 4). Input radiation and temperature data for the models were measured by the NOAA-MFP. Net CO₂ flux was calculated as an average of several (2–6) flights made along the N–S transect during a given temporal interval. For example, if two flights were made between 09.30 and 11.00 hours (one from N–S and one return flight from S–N), then measured and scaled net CO₂ flux was calculated as an average of these two flights. Measured and scaled net CO₂ flux was presented as mean values ($\pm 1SE$ and $\pm 90\%$ CI) calculated for each flight campaign (June 1994, $n=7$; June and August 1995, $n=4$).

Results

Kuparuk basin net CO₂ flux

The availability of climatic and satellite-derived data allows the field data to be scaled to the Kuparuk River Basin in a continuous fashion throughout the year. Acidic and shrub tundra surfaces of the Kuparuk Basin

were net sources of the CO₂ to the atmosphere of 300–400 kgC km⁻² d⁻¹ (0.3–0.4 gC m⁻² d⁻¹) during the snow-melt period (May–June) of the 1995 growing season (positive values denote net CO₂ emission; Fig. 5a). Non-acidic tundra ecosystems were net sources of 150 kgC km⁻² d⁻¹ and wet-sedge tundra was approximately in balance (Fig. 5a). A N–S gradient in cumulative daily net CO₂ emission was apparent by mid-June, as the moist-acidic and shrub tundra dominated southern portion of the Kuparuk basin exhibited larger cumulative net CO₂ loss (Fig. 6a). The northern portion of the Kuparuk basin was a smaller cumulative net source in early June, due to the predominance of nonacidic and wet sedge surface types which exhibited relatively lower rates of daily net CO₂ loss (Fig. 5a). The combined net efflux of the Kuparuk basin was 200–300 kgC km⁻² d⁻¹ between May and June (Fig. 5b).

Following snowmelt, daily rates of net CO₂ efflux declined in all tundra surfaces, and by 1 July, net CO₂ flux was on average –250 kgC km⁻² d⁻¹ for acidic and nonacidic tundra (Fig. 5a). Wet sedge was only a small sink (–50 kgC km⁻² d⁻¹) by 1 July, while daily rates of net CO₂ loss in shrub tundra decreased to nearly 50 kgC km⁻² d⁻¹ by late-June (Fig. 5a). The strong N–S gradient in cumulative daily net CO₂ uptake was apparent by 15 July, as approximately 10 gC m⁻² had accumulated in nonacidic tundra ecosystems of the coastal plain, while 10–40 gC m⁻² had been lost from acidic and shrub tundra surfaces of the foothills (Fig. 6b). Because moist-acidic and nonacidic tundra comprised the majority of the terrestrial surface area of the Kuparuk River Basin (e.g. 74%), the daily net CO₂ flux for the Kuparuk Basin was nearly –150 kgC km⁻² d⁻¹ by 1 July (Fig. 5b).

Daily rates of net CO₂ uptake for acidic, nonacidic, and wet-sedge tundra continued to increase throughout July (Fig. 5a). By 1 August, daily net CO₂ flux for acidic and nonacidic tundra ecosystems was –600 and –300 kgC km⁻² d⁻¹, respectively, while wet-sedge net CO₂ flux was –100 kgC km⁻² d⁻¹ (Fig. 5a). Shrub tundra ecosystems exhibited a brief increase in net CO₂ loss in the beginning of July (e.g. 175 kgC km⁻² d⁻¹), but by 1 August shrub tundra ecosystems were net sinks of –100 kgC km⁻² d⁻¹ (Fig. 5a). By mid-August, nonacidic tundra-dominated portions of the northern Kuparuk Basin (cool colours) had accumulated nearly 40 gC m⁻², but in the foothills region, cumulative net CO₂ flux was spatially variable with large areas of cumulative net uptake (acidic tundra) adjacent to large areas of cumulative net loss (shrub-tundra) (Fig. 6c). Whole-basin rates of daily net CO₂ flux increased from –150 kgC km⁻² d⁻¹ in early July to a seasonal peak of –300 kgC km⁻² d⁻¹ by 1 August (Fig. 5b).

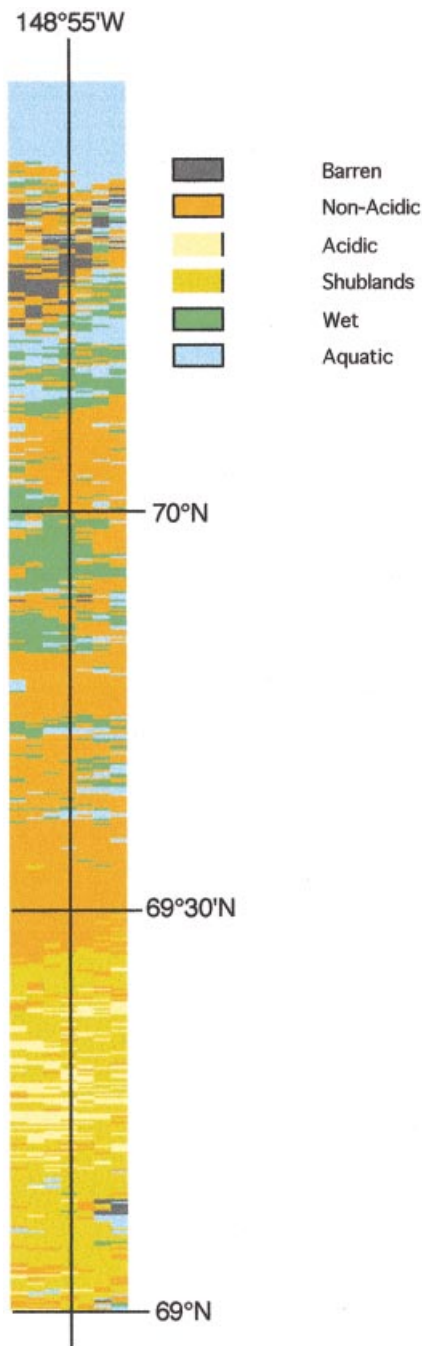


Fig. 4 Landscape surface map for the 148°55'W NOAA aircraft flux measurement transect. Landscape surface features obtained from the Kuparuk Basin landscape surface map (see Fig. 1; Auerbach & Walker 1995; Auerbach *et al.* 1997) were spatially distributed within a ± 1 km belt transect centred on the 140 km long flightline transect (solid vertical line).

Daily rates of net CO_2 assimilation decreased in nonacidic, acidic, and wet-sedge tundra toward the end of August (Fig. 5a), and as a result, the rate of whole-basin daily net CO_2 uptake declined as well (Fig. 5b). By

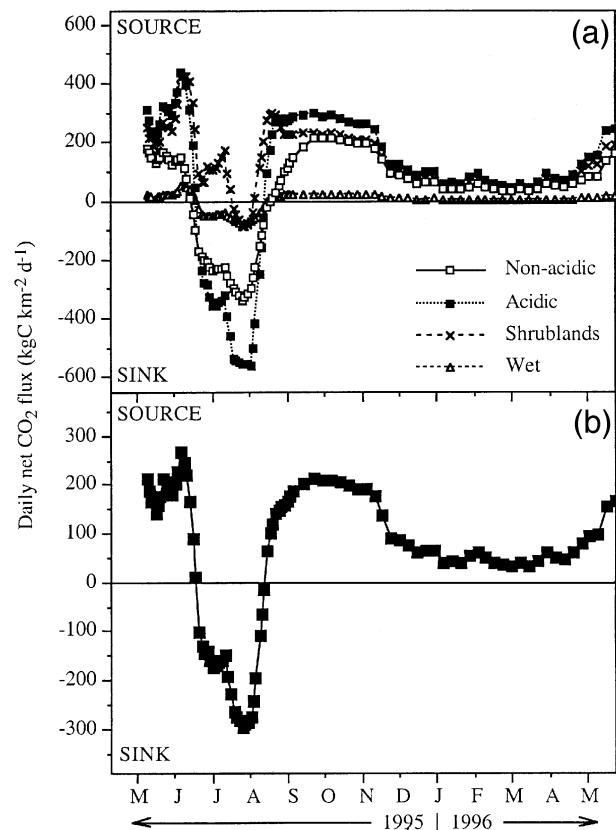


Fig. 5 (a) Total daily integrated net CO_2 flux for the nonacidic (open boxes, solid lines), acidic (closed boxes, solid lines), shrub (crosses, dashed lines), and wet sedge (open triangles, dashed lines) surfaces of the Kuparuk River Basin during the 1995–96 annual cycle. (b) Integrated net CO_2 flux for the entire Kuparuk River Basin for the 1995–96 annual cycle.

early September, all vegetation types were net sources of CO_2 , with 25–100 $\text{kgC km}^{-2} \text{d}^{-1}$ emitted from nonacidic and wet tundra and 200–300 $\text{kgC km}^{-2} \text{d}^{-1}$ from acidic and shrub tundra (Fig. 5a). The N–S pattern of cumulative net CO_2 flux observed on 15 August (Fig. 6c) was substantially different on 15 September (Fig. 6d), with the largest cumulative uptake occurring in nonacidic surfaces and the largest cumulative loss occurring in the shrub-tundra dominated surfaces. Whole-basin rates of daily net CO_2 flux at the end of the growing season (6 September) were nearly 200 $\text{kgC km}^{-2} \text{d}^{-1}$ (Fig. 5b).

Daily rates of fall and winter net CO_2 efflux were largest for acidic tundra ecosystems and lowest for wet-sedge tundra (Fig. 5a). Daily net CO_2 flux for the September–November period was 200–300 $\text{kgC km}^{-2} \text{d}^{-1}$ for acidic, nonacidic, and shrub tundra, 25 $\text{kgC km}^{-2} \text{d}^{-1}$ for wet-sedge tundra, and 200–250 $\text{kgC km}^{-2} \text{d}^{-1}$ for the Kuparuk Basin (Fig. 5a & b). After November, daily rates of net efflux decreased substantially for all vegetation

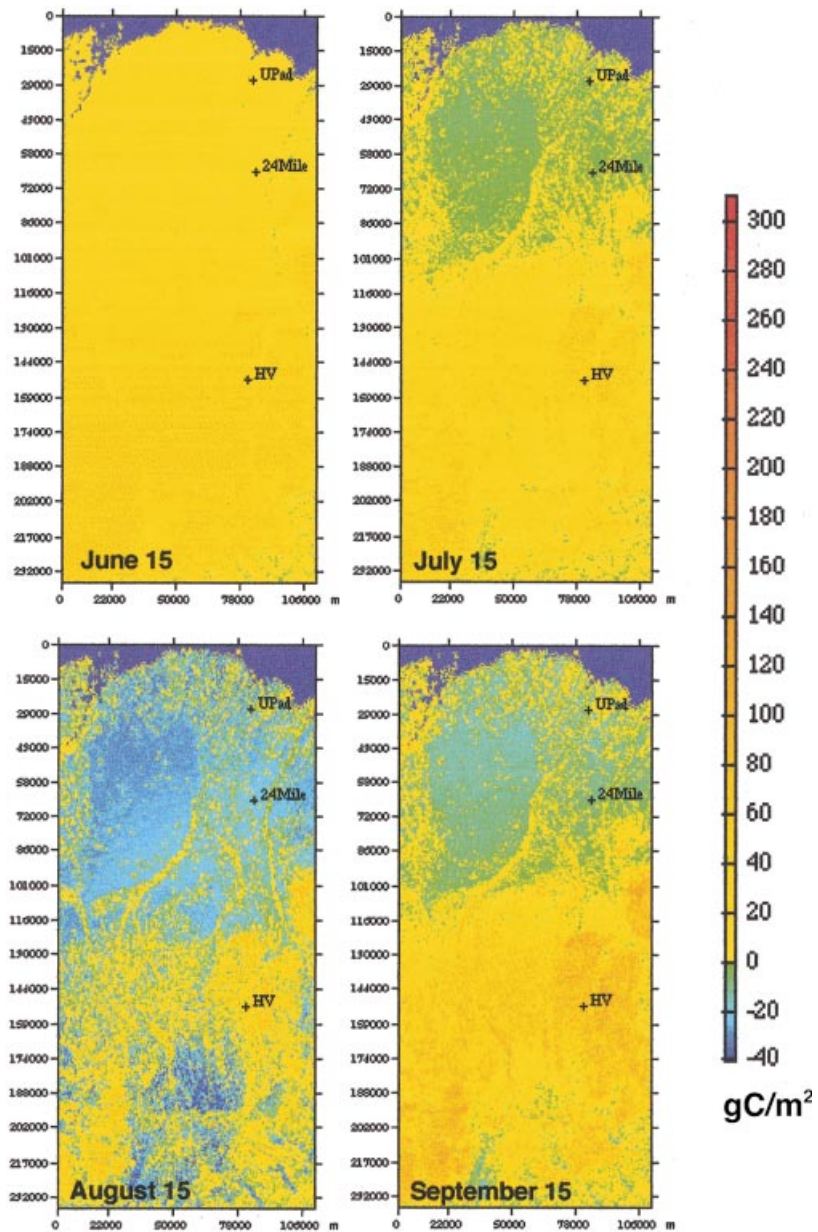


Fig. 6 Cumulative net CO₂ flux for the Kuparuk River Basin on (a) 15 June, (b) 15 July, (c) 15 August and (d) 15 September 1995. Data were generated using a GIS consisting of daily net CO₂ flux models, landscape surface map, bi-monthly NDVI composites, and spatially distributed radiation and temperature fields. Also plotted for reference are the locations of the Happy Valley, 24-Mile, and U-Pad study sites.

types due to a seasonal decline in soil temperatures. Net CO₂ flux for acidic, shrub, and nonacidic tundra was 50–75 kgC km⁻² d⁻¹ during the December–April winter period, while wet-sedge tundra emitted only about 10–20 kgC km⁻² d⁻¹ over the winter (Fig. 5a). However, whole-basin CO₂ efflux remained relatively high during the winter period (e.g. 50–100 kgC km⁻² d⁻¹) due to the combined efflux from the individual land-cover types (Fig. 5b). After April, net efflux increased due to an increase in soil temperature, and by 1 May, net efflux reached a value of 100 kgC km⁻² d⁻¹ for the acidic, nonacidic, and shrub tundra ecosystems (Fig. 5a). Wet-

sedge tundra efflux increased only slightly over the same period, but the combined efflux from the land-cover types resulted in a substantial increase in whole-basin net CO₂ emission (100 kgC km⁻² d⁻¹ by 1 May; Fig. 5b).

When integrated for the summer growing season (9 May–5 September), nonacidic tundra was a net sink of -31.7 ± 21.3 GgC (1 GgC = 10⁹ gC), while acidic and wet sedge tundra surfaces were approximately in balance (negative values denote net ecosystem CO₂ uptake; Table 2). Shrub tundra lost 32.5 ± 6.3 GgC over the summer growing season, and whole basin summer net CO₂ exchange was estimated to be -0.9 ± 50.3 GgC

(Table 2). Integrated fall and winter (6 September–8 May) net CO₂ flux was estimated to be 75.5 ± 8.3 GgC for acidic tundra, 96.4 ± 11.4 GgC for nonacidic tundra, 43.3 ± 4.7 GgC for shrublands, 1.4 ± 0.2 GgC for wet sedge tundra, and 217.2 ± 24.1 GgC for the entire Kuparuk Basin (Table 2). Acidic, nonacidic, and shrub tundra were comparable net sources of CO₂ to the atmosphere over the annual cycle (i.e. 64.7–75.8 GgC), while wet sedge tundra was roughly in balance (Table 2). The Kuparuk River Basin was a net source of 218.1 ± 60.6 GgC for the 1995–96 annual cycle (Table 2).

Performance of the scaling procedure

Scaled estimates of net CO₂ exchange compared well with measured values obtained from the NOAA-MFP, and in general, measured rates of net CO₂ flux over the latitudinal transect exhibited larger spatial variability than the scaled values (Fig. 7). During the June 1994 flight campaign (Fig. 7a), measured net CO₂ flux in the extreme southern portion of the flux transect (69°00'N) ranged between -0.1 and -0.05 mgCO₂ m⁻² s⁻¹ (negative values denote net ecosystem CO₂ uptake) while scaled net CO₂ flux was on average -0.05 mgCO₂ m⁻² s⁻¹. Measured and scaled rates of net CO₂ uptake near 69°15'N were similar (-0.10 mgCO₂ m⁻² s⁻¹), but between 69°15'N–69°30'N, measured rates of net CO₂ uptake were 0.05–0.1 mgCO₂ m⁻² s⁻¹ larger than the scaled values (Fig. 7a). However, because of the large spatial variability in measured net CO₂ flux (expressed as a ± 90% confidence interval), the scaled values were generally within the observed variance (Fig. 7a). Measured and scaled rates of net CO₂ flux were on average -0.10 mgCO₂ m⁻² s⁻¹ near the boundary between acidic and nonacidic tundra

(69°30'N), and net CO₂ uptake gradually decreased north of the foothills-coastal plain transition (Fig. 7a). Measured and scaled rates of net CO₂ flux were approximately -0.05 mgCO₂ m⁻² s⁻¹ along the coastal plain (69°30'N–70°00'N) and -0.025 mgCO₂ m⁻² s⁻¹ near the arctic coast (70°15'N) (Fig. 7a). When averaged across the N–S transect, scaled net CO₂ flux (± 1SE) for the June 1994 campaign was -0.059 ± 0.033 mgCO₂ m⁻² s⁻¹ while measured net CO₂ flux was -0.088 ± 0.023 mgCO₂ m⁻² s⁻¹ (Fig. 8).

Compared to the June 1994 campaign (Fig. 7a), the correspondence between the measured and scaled fluxes in June 1995 was relatively higher in the foothills region (69°00'N–69°22'N) and lower along the coastal plain (69°30'N–70°15'N) (Fig. 7b). The divergence in measured and scaled rates of net CO₂ flux observed near 69°30'N in June 1994 (Fig. 7a) persisted in June 1995; however, the latitudinal extent and the magnitude of the divergence was substantially smaller than in June 1994 (Fig. 7b). The variance in the measured values (e.g. ± 90% confidence interval) was also smaller in June 1995 (Fig. 7b), lending more confidence in both the measured flux value and the performance of the scaling procedure. When averaged for the entire flux transect, measured net CO₂ flux (± 1SE) was 0.037 ± 0.021 mgCO₂ m⁻² s⁻¹ and scaled net CO₂ flux was 0.037 ± 0.013 mgCO₂ m⁻² s⁻¹ (Fig. 8).

The N–S gradient in net CO₂ uptake observed during the June campaigns was reversed in August, as rates of CO₂ uptake were relatively larger along the arctic coastal plain (Fig. 7c). Scaled net CO₂ flux was c. -0.05 mgCO₂ m⁻² s⁻¹ between 69°30'N–70°15'N, while measured flux ranged between 0 and -0.125 mgCO₂ m⁻² s⁻¹ (Fig. 7c). Scaled net CO₂ flux near the foothills-coastal plain transition was nearly -0.1 mgCO₂ m⁻² s⁻¹, which was comparable to the average measured value

Table 2 Seasonal (summer and winter) and annual net CO₂ flux for the land-cover types and the Kuparuk River Basin, Alaska during 1995–96 (1 Gg of C = 10⁹ gC). Data represent bootstrapped estimates of the total seasonal and annual (± 1SE) net CO₂ flux calculated from 4000 iterations

Surface type	Area (km ²)†	Summer‡ (gC m ⁻²)	Winter§ (gC m ⁻²)	Annual (gC m ⁻²)	Summer† (Gg C)	Winter§ (Gg C)	Annual (Gg C)
Acidic	2250	-4.1 ± 9.9	33.6 ± 3.7	29.5 ± 11.3	-9.1 ± 22.2	75.5 ± 8.3	66.4 ± 25.5
Non-acidic	4163	-7.6 ± 5.1	23.2 ± 2.7	15.6 ± 7.0	-31.7 ± 21.3	96.4 ± 11.4	64.7 ± 29.2
Shrub	1620	20.1 ± 3.9	26.7 ± 2.9	46.8 ± 5.2	32.5 ± 6.3	43.3 ± 4.7	75.8 ± 8.4
Wet sedge	574	-1.7 ± 1.1	2.3 ± 0.3	0.6 ± 1.3	-1.0 ± 0.7	1.4 ± 0.2	0.4 ± 0.8
Aquatic	464	19.1 ± 1.6	0.9 ± 0.9	20.0 ± 4.1	8.9 ± 0.8	3.6 ± 3.6	12.5 ± 1.9
Barren	129	0.0 ± 0.0	0.0 ± 0.0	0.0 ± 0.0	0.0 ± 0.0	0.0 ± 0.0	0.0 ± 0.0
Basin total	9200	-0.1 ± 5.5	23.6 ± 2.6	23.5 ± 6.5	-0.9 ± 50.3	217.2 ± 24.1	218.1 ± 60.6

†Area for the land-cover types is from Auerbach *et al.* (1997).

‡ Summer refers to the period between 9 May and 5 September 1996.

§ Winter refers to the period between 6 September 1996 and 8 May 1997.

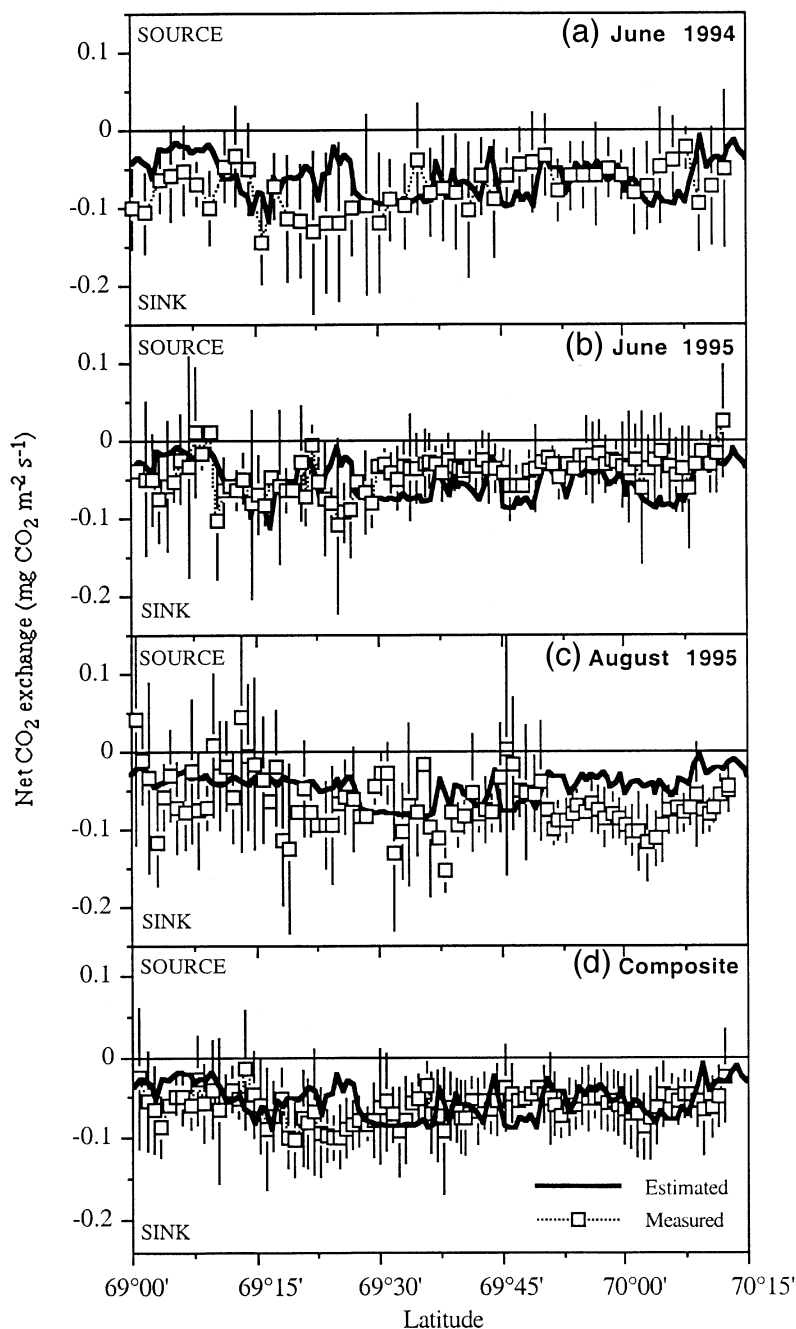


Fig. 7 Scaled (solid lines) and measured (open boxes) net CO₂ flux along the 148°55'W aircraft flux measurement transect during the June 1994 (a), June 1995 (b), August 1995 (c), and composite average of all campaigns (d). Scaled net CO₂ flux was calculated from instantaneous models (eqns 1 and 2) driven by radiation and temperature measured directly by the NOAA-MFP for each terrestrial vegetation type within the 2 km-wide and a 140 km-long aircraft transect (Fig. 4). Measured fluxes correspond to aircraft-based eddy covariance measurements made by the NOAA flux aircraft (see Methods). Data correspond to means calculated from 4 to 7 complete transect measurements (each consisting of 4–6 one-way flights along the flux transect) conducted during each flight campaign (e.g. June 1994 and 1995, August 1995), while the composite (d) corresponds to an average of the three flight campaigns. Error bars depict the $\pm 90\%$ confidence interval for the averaged measured flux.

(Fig. 7c). Scaled net CO₂ flux in the foothills region was on average $-0.025 \text{ mgCO}_2 \text{ m}^{-2} \text{ s}^{-1}$ while measured net CO₂ flux ranged from $+0.05$ to $-0.10 \text{ mgCO}_2 \text{ m}^{-2} \text{ s}^{-1}$ (Fig. 7c). The average scaled net CO₂ flux ($\pm 1\text{SE}$) for the transect was $-0.039 \pm 0.009 \text{ mgCO}_2 \text{ m}^{-2} \text{ s}^{-1}$, while the measured value was $-0.064 \pm 0.007 \text{ mgCO}_2 \text{ m}^{-2} \text{ s}^{-1}$ (Fig. 8).

When averaged over all aircraft campaigns, the correspondence between the scaled and measured net CO₂ flux along the latitudinal transect was close, and

only about 14% of the scaled values were outside the $\pm 90\%$ confidence intervals (Fig. 7d). Measured and scaled net CO₂ flux for the foothills region (69°00'N–69°30'N) was on average $-0.05 \text{ mgCO}_2 \text{ m}^{-2} \text{ s}^{-1}$ (Fig. 7d). North of the foothills–coastal plain transition (69°30'N), scaled and measured fluxes ranged between -0.05 and $-0.10 \text{ mgCO}_2 \text{ m}^{-2} \text{ s}^{-1}$, while net CO₂ flux in the wet sedge and aquatic ecosystems along the arctic coast was $-0.025 \text{ mgCO}_2 \text{ m}^{-2} \text{ s}^{-1}$ (Fig. 7d). Average scaled and

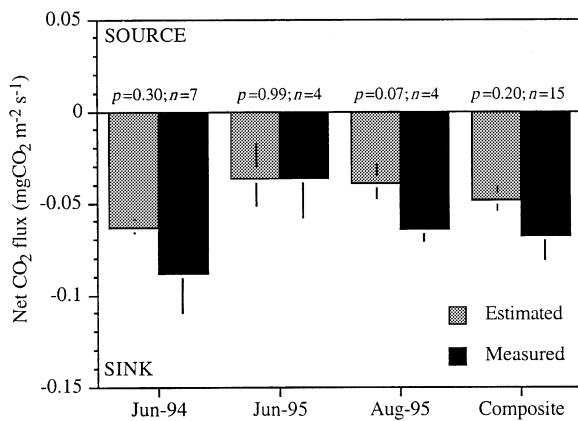


Fig. 8 Average estimated (stippled columns) and measured (solid columns) net CO₂ flux along the 148°55'W latitudinal transect during the individual flight 1994–95 flight campaigns, and averaged over all flight campaigns (composite). Numbers displayed over each set of columns refer to the comparison-wise probability (*p*) of committing a type-I error using a two-tailed *t*-test, and the number of complete transect measurements (*n*) used in each *t*-test. Data are means ± 1SE, *n* = 7 (June 1994), 4 (June and August 1995), and 15 (composite).

measured net CO₂ flux (± 1SE) for the composite transect was -0.048 ± 0.005 and -0.068 ± 0.013 mgCO₂ m⁻² s⁻¹, respectively (Fig. 8).

Discussion

The minimum data requirements of the GIS-based approach described here allow for the rapid and convenient scaling of plot- and landscape-scale measurements of net CO₂ flux to the watershed and regional scales. The approach is unique in that it scales a process (e.g. net CO₂ flux as a function of seasonal ecosystem development and meteorology) instead of extrapolating ground-based measurements to the regional scale. This property is important because it accounts for the substantial spatial and temporal variability in vegetation composition, ecosystem development, and meteorology (surface temperature and radiation) observed across arctic regions (Weller *et al.* 1995; Auerbach *et al.* 1997). For example, area-integrated measurements of net CO₂ flux derived from tower-based eddy covariance indicate that the Prudhoe Bay, U-Pad wet sedge tundra ecosystem was a net CO₂ sink of -16 gC m⁻² during the 1995 summer growing season (Vourlitis & Oechel 1997). By simple extrapolation, multiplying this value by the area of wet sedge tundra in the Kuparuk basin (574 km²) yields a summer net CO₂ flux estimate of -9.2 GgC, which is roughly nine times larger than the scaled estimate calculated from the Kuparuk-GIS ($-1.0 +$

0.7 GgC; Table 2). This large discrepancy occurs despite the fact that the model used to derive the scaled estimate of summer net CO₂ flux for wet sedge tundra was parameterized from the 1995 U-Pad data. At the other end of the spectrum, more complicated simulation approaches may yield similar results to the GIS-based approach reported here, but the data required to parameterize and run these simulations are not likely to be available at the regional scale (Raich *et al.* 1991; Williams *et al.* 1997).

The limited comparisons between the scaled and aircraft-measured values of net CO₂ flux suggest that the spatial and temporal scaling procedure provided realistic estimates of net CO₂ exchange for the Kuparuk River Basin (see Figs 7 and 8). However, the approach has several potential sources of uncertainty that must be considered. For example, fall and winter flux estimates, which are based on limited chamber flux measurements made during the 1993–94 winter season (Oechel *et al.* 1997), were not assessed due to the difficulty of operating the NOAA-MFP during cold and dark winter periods. Because the estimated efflux over the winter period fully compensates for the summer sink activity, resulting in a net loss of CO₂ from the Kuparuk basin over the annual cycle, the autumn and winter basin-scale flux estimates must be considered with caution. However, the magnitude of the winter efflux estimated for the Kuparuk Basin is conservative compared to fluxes reported for a variety of Alaskan arctic tundra ecosystems (Zimov *et al.* 1996; Oechel *et al.* 1997; Fahnestock *et al.* 1998). Other sources of uncertainty include the aquatic ecosystem contribution to regional net CO₂ flux. Although our approach is based on data reported by Kling *et al.* (1991), which represents the most authoritative study on aquatic CO₂ flux in arctic Alaska, the net CO₂ exchange of aquatic ecosystems will undoubtedly be estimated with greater certainty as more data become available.

Another source of uncertainty lies in the characterization of the vegetation cover types represented in the GIS land-cover layer for the Kuparuk River watershed. Field studies of randomly selected plots within the Kuparuk Basin indicate that the landcover map had 87% accuracy (Auerbach *et al.* 1997; Muller *et al.* 1998). However, errors in land-cover classification were apparent near, for example, Happy Valley where the land-cover map indicated predominantly shrub tundra while the vegetation was more characteristic of acidic tussock tundra (D. A. Walker, University of Colorado, pers. comm.). Since the vegetation layer is central to our spatial scaling approach, discrepancies between mapped and actual vegetation may produce erroneous estimates of net CO₂ flux for specific portions of the Kuparuk basin.

Other potential sources of error include failure to estimate the sample footprint of the NOAA-MFP. The

sample footprint of the NOAA-MFP is a complex function of the measurement height, wind speed and direction, and thermal stability (Leclerc & Thurtell 1990; Schuepp *et al.* 1990; Crawford *et al.* 1996), and as a result, the surface features contributing to the measured flux are spatially and temporally variable. Failure to simulate the meandering of the sample footprint can lead to mis-registration of the vegetation contributing to the scaled flux, and thus, discrepancies between the scaled and measured net CO₂ flux value (Austin *et al.* 1987; Crawford *et al.* 1996; Oechel *et al.* 1998).

Problems associated with aircraft flux measurement may have also been responsible for divergence between the measured and scaled net CO₂ flux values. The southern portion of the flux transect was in the foothills region of the Brooks Range, and consisted of gently rolling hills and broad river valleys. In the northern portion, the transect crossed into the Prudhoe Bay oil field where venting and flaring of CH₄ gas trapped in the extracted crude oil periodically resulted in an enriched atmospheric CO₂ plume (Brooks *et al.* 1997). Although large departures (typically order of magnitude) in aircraft net CO₂ flux were removed from analysis, the complex terrain and gas flaring could have increased the spatial variance in the aircraft-derived net CO₂ flux.

The scaling approach worked well for the Kuparuk River basin, where extensive measurement and spatial characterization studies were conducted. Recent research indicates that the spatial variations in vegetation cover types characterized by the land-cover layer corresponded closely to spatial patterns in the NDVI (Stow *et al.* 1998). Thus, use of NDVI maps derived from NOAA-AVHRR imagery and/or similar satellite platforms will allow this approach to be utilized in regions where detailed vegetation maps are currently lacking. Similarly, Synthetic Aperture Radar (SAR) imagery appears to be sensitive to the spatial and temporal variations in surface water content (Kane *et al.* 1996). Because soil water content alters rates of microbial decomposition and net CO₂ exchange (Bunnell *et al.* 1977; Billings *et al.* 1982; Oechel *et al.* 1993, 1995; Funk *et al.* 1994; Oechel & Vourlitis 1995; Johnson *et al.* 1996), SAR imagery offers a means for refining regional estimates of *R*. With these improvements, this simple scaling approach will be useful for estimating the net CO₂ exchange of arctic Alaska.

Acknowledgements

This research was supported by the National Science Foundation, Arctic Systems Science, Land-Atmosphere-Ice-Interactions Program (OPP-9216109). Logistic support was provided by personnel from the Polar Ice Coring Office of the University of Alaska, Fairbanks (1994) and the University of Nebraska, Lincoln (1995–96), Institute of Arctic Biology,

University of Alaska, Fairbanks, and the Piquiniq Management Corporation and the North Slope Borough. Field assistance from Richard Ault, Pablo Bryant, and Steve Hastings of San Diego State University (SDSU), and Melissa Vourlitis are gratefully acknowledged. The authors thank Tilden Meyers and Robert McMillen (NOAA-ATDD), Tagir Gilmanov (Utah State University), and Yoshinobu Harazono (Japan, NIAES) for providing technical expertise.

References

- Auerbach NA, Walker DA (1995) *Preliminary Landsat-derived vegetation map of the Kuparuk River basin, Alaska*. Institute of Arctic and Alpine Research, University of Colorado, Boulder, CO.
- Auerbach NA, Walker DA, Bockheim JG (1997) *Land cover map of the Kuparuk River basin, Alaska*. Institute of Arctic and Alpine Research, University of Colorado, Boulder, CO.
- Austin LB, Schuepp PH, Desjardins RL (1987) The feasibility of using airborne CO₂ flux measurements for the imaging of the rate of biomass production. *Agricultural and Forest Meteorology*, **39**, 13–23.
- Baldocchi D, Valentini R, Running S, Oechel W, Dahlman R (1996) Strategies for measuring and modeling carbon dioxide and water vapor fluxes over terrestrial ecosystems. *Global Change Biology*, **2**, 101–110.
- Billings WD, Peterson KM, Shaver GR, Trent AW (1977) Root growth, respiration, and carbon dioxide evolution in an arctic tundra soil. *Arctic and Alpine Research*, **9**, 129–137.
- Billings WD, Luken JO, Mortensen DA, Peterson KM (1982) Arctic tundra: a source or sink for atmospheric carbon dioxide in a changing environment? *Oecologia*, **53**, 7–11.
- Brooks SB, Crawford TL, Oechel WC (1997) Measurement of carbon dioxide emissions plumes from Prudhoe Bay, Alaska oil fields. *Journal of Atmospheric Chemistry*, **27**, 197–207.
- Bunnell FL, Tait DEN, Flanagan PW, Van Cleve K (1977) Microbial respiration and substrate weight loss. I. A general model of the influences of abiotic variables. *Soil Biology and Biochemistry*, **9**, 33–40.
- Chapin FS III, Shaver GR, Giblin AE, Nadelhoffer KJ, Laundre JA (1995) Responses of arctic tundra to experimental and observed changes in climate. *Ecology*, **76**, 694–711.
- Crawford TL, McMillen RT, Dobosy RJ (1990) Description of a 'Generic' Mobile Flux Platform using a small airplane. *NOAA Technical Memorandum ERL ARL-184*, 81 pp.
- Crawford TL, Dobosy RJ (1992) A sensitive fast-response probe to measure turbulence and heat flux from any airplane. *Boundary-Layer Meteorology*, **59**, 257–278.
- Crawford TL, Dobosy RJ, McMillen RT, Vogel CA, Hicks BB (1996) Air-surface exchange measurement in heterogeneous regions: extending tower observations with spatial structure observed from small aircraft. *Global Change Biology*, **2**, 275–286.
- Desjardins RL, Schuepp PH, MacPherson JI, Buckley DJ (1992) Spatial and temporal variations of the fluxes of carbon dioxide and sensible and latent heat over the FIFE site. *Journal of Geophysical Research*, **97**, 18,467–18,475.
- Efron B, Tibshirani R (1993). *An Introduction to the Bootstrap*. Chapman & Hall, New York.
- Fahnestock JT, Jones MH, Brooks PD, Walker DA, Welker JM (1998) Winter and early spring CO₂ efflux from tundra

- communities of northern Alaska. *Journal of Geophysical Research*, **103**, 29,023–29,028.
- Funk DW, Pullman ER, Peterson KM, Crill PM, Billings WD (1994) Influence of water table on carbon dioxide, carbon monoxide, and methane fluxes from taiga bog microcosms. *Global Biogeochemical Cycles*, **8**, 271–278.
- Grulke NE, Riechers GH, Oechel WC, Hjelm U, Jaeger C (1990) Carbon balance in tussock tundra under ambient and elevated atmospheric CO₂. *Oecologia*, **83**, 485–494.
- Hinzman LD, Goering DJ, Kane DL (1998) A distributed thermal model for calculating soil temperature profiles of depth of thaw in permafrost regions. *Journal of Geophysical Research*, **103**, 28,975–28,992.
- Hope AS, Kimball JS, Stow DA (1993) The relationship between tussock tundra spectral reflectance properties and biomass and vegetation composition. *International Journal of Remote Sensing*, **14**, 1861–1874.
- Hope AS, Fleming JB, Vourlitis GL, Stow DA, Oechel WC, Hack T (1995) Relating CO₂ fluxes to spectral vegetation indices in tundra landscapes: Importance of footprint definition. *Polar Record*, **31**, 245–250.
- Johnson LC, Shaver GR, Giblin AE *et al.* (1996) Effects of drainage and temperature on carbon balance of tussock tundra microcosms. *Oecologia*, **108**, 737–748.
- Kane DL, Hinzman LD, Yu H, Goering DJ (1996) The Use of SAR Satellite Imagery to Measure Active Layer Moisture Contents in Arctic Alaska. *Nordic Hydrology*, **27**, 25–38.
- Kicklighter DW, Melillo JM, Peterjohn WT, Rastetter EB, McGuire AD, Steudler PA (1994) Aspects of spatial and temporal aggregation in estimating regional carbon dioxide fluxes from temperate forest soils. *Journal of Geophysical Research*, **99** (D1), 1303–1315.
- Kling GW, Kipphut GW, Miller MC (1991) Arctic lakes and streams as conduits to the atmosphere: Implications for tundra carbon budgets. *Science*, **251**, 298–301.
- Leclerc MY, Thurtell GW (1990) Footprint prediction of scalar fluxes using Markovian analysis. *Boundary Layer Meteorology*, **52**, 247–258.
- McMichael CE (1995) *Estimating CO₂ exchange in arctic tundra ecosystems using a spectral vegetation index*. Master's Thesis, San Diego State University.
- McMichael CE, Hope AS, Stow DA, Vourlitis G, Oechel W, Fleming J (1999) Estimating Carbon fluxes on the north slope of Alaska using a spectral vegetation index. *International Journal of Remote Sensing*, **20**, 683–698.
- Muller SV, Walker DA, Auerbach NA, Guyer S, Sherba D, Bockheim J, Nelson F (1998) Accuracy assessment of a land-cover map of the Kuparuk River basin, Alaska: Considerations for remote regions. *Photogrammetric Engineering and Remote Sensing*, **64**, 619–628.
- Oechel WC, Hastings SJ, Vourlitis GL, Jenkins M, Riechers G, Grulke N (1993) Recent Change of Arctic tundra ecosystems from a net carbon dioxide sink to a source. *Nature*, **361**, 520–523.
- Oechel WC, Vourlitis GL (1994) The effects of climate change on land-atmosphere feedbacks in arctic tundra regions. *Trends in Ecology and Evolution*, **9**, 324–329.
- Oechel WC, Vourlitis GL (1995) Effects of global change on carbon storage in cold soils. In: *Advances in Soil Science: Soils and Global Change* (Lal R *et al.*, eds), pp. 117–129. Lewis Publishers, Boca Raton, FL.
- Oechel WC, Vourlitis GL, Hastings SJ, Bochkarev SA (1995) Change in carbon dioxide flux at the U.S. Tundra International Biological Program Sites at Barrow, AK. *Ecological Applications*, **5**, 846–855.
- Oechel WC, Hastings SJ, Vourlitis GL (1997) Cold season CO₂ emission from arctic soils. *Global Biogeochemical Cycles*, **11**, 163–172.
- Oechel WC, Brooks SB, Vourlitis GL, Crawford TL, Dumas EJ (1998) Intercomparison between chamber, tower, and aircraft net CO₂ exchange and energy fluxes measured during the Arctic Systems Science Land-Atmosphere-Ice-Interactions (ARCSS-LAI) flux study. *Journal of Geophysical Research*, **103**, 28,993–28,004.
- Peterson KM, Billings WD (1975) Carbon dioxide flux from tundra soils and vegetation as related to temperature at Barrow. *Alaska The American Midland Naturalist*, **94**, 88–98.
- Raich JW, Rastetter EB, Melillo JM *et al.* (1991) Potential net primary productivity in South America: application of a global model. *Ecological Applications*, **1**, 399–429.
- Rastetter EB, King AW, Crosby BJ, Hornberger GM, O'Neill RV, Hobbie JE (1992) Aggregating fine-scale ecological knowledge to model coarser-scale attributes of ecosystems. *Ecological Applications*, **2**, 55–70.
- Rastetter EB (1996) Validating models of ecosystem response to global change. *Bioscience*, **46**, 190–198.
- Ruimy A, Jarvis PG, Baldocchi DD, Saugier B (1995) CO₂ fluxes over plant canopies and solar radiation: a review. *Advances in Ecological Research*, **26**, 1–68.
- Schuepp PH, Leclerc MY, MacPherson JJ, Desjardins RL (1990) Footprint prediction of scalar fluxes from analytical solutions of the diffusion equation. *Boundary-Layer Meteorological Journal*, **50**, 355–374.
- Stow D, Hope A, Boynton W, Phinn S, Walker D, Auerbach N (1998) Satellite-Derived Vegetation Index and Cover Type Maps for Estimating Carbon Dioxide Flux for Arctic Tundra Regions. *Geomorphology*, **21**, 313–327.
- Tenhunen JD, Gillespie CT, Oberbauer SF, Sala A, Whalen S (1995) Climate effects on the carbon balance of tussock tundra in the Philip Smith Mountains. *Alaska Flora*, **190**, 273–283.
- Thornley JHM (1976) *Mathematical Models in Plant Physiology*. Academic Press, New York, 312 pp.
- VEMAP Members (1995) Vegetation/ecosystem modeling and analysis project: Comparing biogeography and biogeochemistry models in a continental-scale study of terrestrial ecosystem responses to climate change and CO₂ doubling. *Global Biogeochemical Cycles*, **9** (4), 407–437.
- Vourlitis GL, Oechel WC, Hastings SJ, Jenkins MA (1993) A system for measuring *in situ* CO₂ and CH₄ flux in unmanaged ecosystems: an arctic example. *Functional Ecology*, **7**, 369–379.
- Vourlitis GL, Oechel WC (1997) Landscape-scale CO₂, H₂O vapour, and energy flux of moist-wet coastal tundra ecosystems over two growing-seasons. *Journal of Ecology*, **85**, 575–590.
- Vourlitis GL, Oechel WC (1999) Eddy covariance measurements of CO₂ and energy fluxes of an Alaskan tussock tundra ecosystem. *Ecology*, **80**, 686–701.
- Vourlitis GL, Harazono Y, Oechel WC, Yoshimoto M, Mano M (2000a) Spatial and temporal variations in hectare-scale net CO₂ flux, respiration, and gross primary production of arctic tundra ecosystems. *Functional Ecology*, in press.
- Vourlitis GL, Oechel WC, Hope A *et al.* (2000b) Physiological models for scaling plot-scale measurements of CO₂ flux across an arctic tundra landscape. *Ecological Applications*, **10**, 60–72.

- Weller G, Chapin FS III, Everett KR *et al.* (1995) The Arctic Flux Study: a regional view of trace gas release. *Journal of Biogeography*, **22**, 365–374.
- Williams RS, Hall DK (1993) Glaciers. In: *Atlas of Satellite Observations Related to Global Change* (Gurney RJ *et al.*, eds), pp. 401–424. Cambridge University Press, Cambridge.
- Williams M, Rastetter EB, Fernandes DN, Goulden ML, Shaver GR, Johnson LC (1997) Predicting gross primary productivity in terrestrial ecosystems. *Ecological Applications*, **7** (3), 882–894.
- Zimov SA, Davidov SP, Voropaev YV *et al.* (1996) Siberian CO₂ efflux in winter as a CO₂ source and cause of seasonality in atmospheric CO₂. *Climate Change*, **33**, 111–120.